Crystal Structure and Spectroscopic and Magnetic Properties of the Manganese(II) and Copper(II) Azido−Tetramethylammonium Systems

Franz A. Mautner,*,† Samy Hanna,† Roberto Cortés,‡ Luis Lezama,§ M. Gotzone Barandika,‡ and Teófilo Rojo*,§

Institut für Physikalische und Theoretische Chemie, Technische Universität Graz, A-8010 Graz, Austria, Departamento de Química Inorgánica, Facultad de Farmacia, Universidad del País Vasco, Apartado 450, E-01080 Vitoria, Spain, and Departamento de Química Inorgánica, Facultad de Ciencias, Universidad del País Vasco, Apartado 644, E-48080 Bilbao, Spain

Received December 1, 1998

The compounds $[N(CH_3)_4][Cu(N_3)_3]$ (**1**) and $[N(CH_3)_4][Mn(N_3)_3]$ (**2**) have been synthesized and characterized. Compound **1** crystallizes in the monoclinic $P2_1/n$ space group, with $Z = 4$, $a = 7.473(2)$ Å, $b = 15.780(2)$ Å, $c = 9.321(2)$ Å, and $\beta = 92.59(2)°$. Compound **2** crystallizes in the monoclinic $P2_1$ space group, with $Z = 2$, $a = 6.264(3)$ Å, $b = 13.150(6)$ Å, $c = 6.375(3)$ Å, and $\beta = 90.00(6)°$. At high temperature, compound **2** undergoes a structural phase transition toward a pseudocubic phase with $a = 6.446(4)$ Å. The nature of the metallic ion remarkably influences the molecular structure of both compounds. Thus, while compound **1** is one-dimensional, with the copper(II) ions bridged by one end-on (EO) and two end-to-end (EE) azido ligands, the structural arrangement in compound **2** is three-dimensional, the manganese(II) ions being bridged by EE azido ligands. In both cases, tetramethylammonium cations stabilize the negative charge of the $[M(N_3)_3]^-$ fragments. Magnetic susceptibility measurements show antiferromagnetic couplings for compounds **1** and **2**. The obtained exchange parameters are $J/k = -3.6$ K, $g = 2.10$ and $J/k = -2.5$ K, $g = 2.01$ for compounds **1** and **2**, respectively.

Introduction

The azido ion has been observed to be a very versatile ligand in bridging different transition metals. In this sense, several dinuclear,[1,2] square planar,[3] and cubane[4] tetranuclear complexes and one-dimensional (1-D),[2b,5,6] two-dimensional (2-D),[7] and three-dimensional (3-D) polymeric complexes[8] have been characterized in which this ligand coordinates by its two possible end-to-end (EE) and end-on (EO) bridging modes. From a magnetic point of view, this variety in structural dispositions results in an interesting area of study. In this respect, it is worth mentioning that the occurrence of antiferromagnetic and ferromagnetic interactions is usually associated with EE[5,6a] and EO bridges,[1,9] respectively. Theoretical calculations have revealed that the singlet and triplet ground states are favored for the EE and EO modes, respectively.

Obtaining three-dimensional (3-D) compounds represents a challenge for researchers in the field of magnetic molecular systems, since it is well-known that one-dimensional systems show no magnetic ordering, except at absolute zero. Therefore, high-dimensional systems are required for extended magnetic ordering to occur. In this sense, the work developed in recent years by our groups on azido-bridged magnetic molecular compounds has led to systems of increasing nuclearity.[6,10]

With this aim, the synthesis plan was focused on the filling of the six vacant coordination sites around the metal ion by azido ligands. Additionally, the use of a relative small positive counterion, such as the tetramethylammonium cation, was thought to be helpful in obtaining 3-D systems. Following this strategy, we successfully isolated a 3-D Mn^{II} compound of the empirical formula $[N(CH_3)_4][Mn(N_3)_3]$. In contrast, the analogously formulated Cu^{II} compound resulted in a one-dimensional system with an unusual disposition of the azido bridges.

Magnetic measurements for both compounds **1** and **2** indicate the occurrence of antiferromagnetic couplings between the copper(II) and manganese(II) ions, respectively. A preliminary communication has been published regarding compound **2**.[10b]

† Technische Universität Graz.
‡ Facultad de Farmacia, Universidad del País Vasco.
§ Facultad de Ciencias, Universidad del País Vasco.

(1) (a) Commarmond, J.; Plumeré, P.; Lehn, J. M.; Agnus, Y.; Louis, R.; Weiss, R.; Kahn, O.; Morgenstern-Badarau, I. *J. Am. Chem. Soc.* **1982**, *104*, 6330. (b) Cortés, R.; Urtiaga, M. K.; Lezama, L.; Larramendi, J. I. R.; Arriortua, M. I.; Rojo, T. *Inorg. Chem.* **1993**, *32*, 3685 and references therein.
(2) (a) Vicente, R.; Escuer, A.; Ribas, J.; El Fallah, M. S.; Solans, X.; Font-Bardía, M. *Inorg. Chem.* **1993**, *32*, 1920. (b) Ribas, J.; Monfort, M.; Diaz, C.; Bastos, C.; Solans, X. *Inorg. Chem.* **1994**, *33*, 484.
(3) Ribas, J.; Monfort, M.; Costa, R.; Solans, X. *Inorg. Chem.* **1993**, *32*, 695.
(4) Halcrow, M. A.; Huffman, J. C.; Christou, G. *Angew. Chem., Int. Ed. Engl.* **1995**, *34*, 889.
(5) (a) Pierpont, C. G.; Hendrickson, D. N.; Duggan, D. M.; Wagner, F.; Barefield, E. K. *Inorg. Chem.* **1975**, *14*, 604. (b) Escuer, A.; Vicente, R.; Ribas, J.; El Fallah, M. S.; Solans, X.; Font-Bardía, M. *Inorg. Chem.* **1993**, *32*, 3727.
(6) (a) Cortés, R.; Urtiaga, M. K.; Lezama, L.; Pizarro, J. L.; Goñi, A.; Arriortua, M. I.; Rojo, T. *Inorg. Chem.* **1994**, *33*, 4009. (b) Cortés, R.; Lezama, L.; Pizarro, J. L.; Arriortua, M. I.; Solans, X.; Rojo, T. *Angew. Chem., Int. Ed. Engl.* **1994**, *33*, 2488.
(7) Cortés, R.; Lezama, L.; Mautner, F. A.; Rojo, T. in *Molecule-Based Magnetic Materials*; Turnbull, M. M., Sugimoto, T., Thomson, L. K., Eds.; American Chemical Society: Washington, DC, 1996; pp 187−200 and references therein.
(8) Escuer, A.; Vicente, R.; Goher, M. A. S.; Mautner, F. A. *Inorg. Chem.* **1996**, *35*, 6386.
(9) Cortés, R.; Pizarro, J. L.; Lezama, L.; Arriortua, M. I.; Rojo, T. *Inorg. Chem.* **1994**, *33*, 2697.
(10) (a) Cortés, R.; Lezama, L.; Pizarro, J. L.; Arriortua, M. I.; Rojo, T. *Angew. Chem., Int. Ed. Engl.* **1996**, *35*, 1810. (b) Mautner, F. A.; Cortés, R.; Lezama, L.; Rojo, T. *Angew. Chem., Int. Ed. Engl.* **1996**, *35*, 78.

10.1021/ic981373s CCC: $18.00
Published on Web 09/18/1999

Experimental Section

Materials. Copper(II) nitrate trihydrate (Aldrich), manganese(II) nitrate (Aldrich), tetramethylammonium hydroxide (Fluka), and sodium azide (Sigma) were purchased and used without further purification.

Synthesis. *Caution!* Azide metal complexes are potentially explosive. Only a small amount of material should be prepared, and it should be handled with caution.

Synthesis of Compounds 1 and 2. The two compounds were prepared similarly by mixing an aqueous solution (20 mL) containing copper(II) nitrate trihydrate (12.1 mg, 0.05 mmol) or manganese(II) nitrate (2.1 g, 8.4 mmol) with a hot aqueous solution of tetramethylammonium azide (45 cm^3, 48 mmol, $T = 340$ K), saturated with hydrazoic acid. Tetramethylammonium azide was prepared by neutralization of an aqueous solution of tetramethylammonium hydroxide with diluted gaseous hydrazoic acid, (HN_3). HN_3 was obtained by adding solid NaN_3 to diluted sulfuric acid (H_2SO_4/H_2O, 1/4 v/v) and transferred by passing a wet air stream through a modified Kipp gas apparatus. Slow evaporation of the resulting clear solutions at room temperature gave black-green needle prism and colorless transparent prism shaped crystals for compounds **1** and **2**, respectively.

$[N(CH_3)_4][Cu(N_3)_3]$ (1). Yield: 55%. Anal. Calcd for $C_4H_{12}N_{10}Cu$: C, 18.22; H, 4.59; N, 53.11. Found: C, 18.15; H, 4.41; N, 52.96. IR (KBr pellets, cm^{-1}): $\nu_{as}(N_3)$ 2100, 2075; $\nu_s(N_3)$ 1300.

$[N(CH_3)_4][Mn(N_3)_3]$ (2). Yield: 60%. Anal. Calcd for $C_4H_{12}N_{10}Mn$: C, 18.83; H, 4.74; N, 54.9. Found: C, 18.68; H, 4.56; N, 54.66. IR (KBr pellets, cm^{-1}): $\nu_{as}(N_3)$ 2105, 2065.

Physical Measurements. IR spectra were recorded on a Nicolet 520 FTIR spectrophotometer in the 400−4000 cm^{-1} region. DSC measurements were carried out in a Perkin-Elmer DSC-7 differential scanning calorimeter with cryogenic equipment, using a cooling/heating rate of 5 °C min^{-1}. Powder X-ray diffraction data were collected with a Philips PW1700 diffractometer, equipped either with a liquid nitrogen chamber (TTK) or with a closed-cycle liquid helium cooling system (He-TTK) (both A. Paar Gmbh, Graz, Austria), Cu Kα radiation, and a secondary monochromator. The X-band EPR measurements, at both low and high temperatures, were carried out on powdered samples with a Bruker ESP 300 spectrometer. Magnetic susceptibilities of powdered samples were carried out in the 1.8−300 K temperature range using a Quantum Design SQUID magnetometer, equipped with a helium continuous-flow cryostat. The magnetic field was approximately 1000 G, a field at which the M vs H curve is linear even for a temperature of 1.8 K. The experimental susceptibilities were corrected for the diamagnetism of the constituent atoms (Pascal's tables).

X-ray Structural Determinations. Diffraction data for **1** and **2** were collected at room temperature on a STOE four-circle automated diffractometer using graphite-monochromated Mo Kα radiation ($\lambda =$ 0.710 69 Å). Crystal data, details of the intensity collection, and some features of the structure refinement for the two compounds are reported in Table 1. Lattice parameters were obtained by a least-squares fit of 42 and 32 reflections in the ranges $11° < 2\theta < 29°$ and $11° < 2\theta < 23°$ for **1** and **2**, respectively. The intensities of three standard reflections were measured every 2 h and showed no significant decrease in intensity.

For compound **1**, 2844 reflections were measured in the range $5° \leq 2\theta \leq 55°$, 1101 of which are assumed as observed for the criterion $I \geq 3\sigma(I)$. For compound **2**, 1373 reflections were measured in the range $5° \leq 2\theta \leq 65°$, 891 of which are considered as observed for the condition $I \geq 4\sigma(I)$. Corrections for Lorentz−polarization and extinction effects were applied for both compounds. An absorption correction was applied for the copper(II) compound. Due to the large number of faces shown by the crystals of this compound, no ideal method could be used and the program DIFABS[11] was applied. Both structures were solved by Patterson syntheses, using SHELXS-86.[12] Afterward, they were refined by full-matrix least-squares methods, using SHELX-76[13] and SHELXL-93[14] computer programs for **1** and **2**, respectively. The twin routine of SHELXL-93 was used (twin matrix: 100, 0$\bar{1}$0, 00$\bar{1}$) for compound **2**. The scattering factors were taken from ref 15. Anisotropic thermal parameters were assigned to all non-hydrogen atoms in both compounds. Constraints were applied to the positions of all hydrogen atoms to which common isotropic temperature factors were assigned. The final R factors were $R(F_o) = 0.049$ ($R_w(F_o) = 0.051$) for compound **1** and $R(F_o) = 0.030$ ($R_w(F_o^2) = 0.069$) for compound **2**. Maximum and minimum peaks in the final difference syntheses were 0.88, −0.76 e $Å^{-3}$ and 0.22, −0.41 e $Å^{-3}$ for compounds **1** and **2**, respectively.

Table 1. Crystal Data and Structure Refinement Details for Compounds **1** and **2**

	1	**2**
empirical formula	$C_4H_{12}N_{10}Cu$	$C_4H_{12}N_{10}Mn$
fw	263.75	255.14
space group	$P2_1/n$ (No. 14)	$P2_1$ (No. 4)
a, Å	7.473(2)	6.264(3)
b, Å	15.780(2)	13.150(6)
c, Å	9.321(2)	6.375(3)
β deg	92.59(2)	90.00(6)
V, $Å^3$	1098.1(4)	525.1(4)
Z	4	2
T, °C	25	25
λ, Å	1.98	1.25
ρ_{obsd}, g cm^{-3}	1.60(2)	1.62(2)
ρ_{calcd}, g cm^{-3}	1.595	1.614
μ, cm^{-1}	19.8	12.5
$R(F_o)^a$	0.049	0.030
$R_w(F_o)^b$	0.051	
$R_w(F_o^2)^c$		0.069

[a] $R(F_o) = \Sigma|\Delta F|/\Sigma|F_o|$. [b] $R_w(F_o) = [\Sigma w(|F_o| - |F_c|)^2/\Sigma w|F_o|^2]^{1/2}$. [c] $R_w(F_o^2) = \{\Sigma[w(\Delta F^2)^2]/\Sigma[w(F_o^2)^2]\}^{1/2}$.

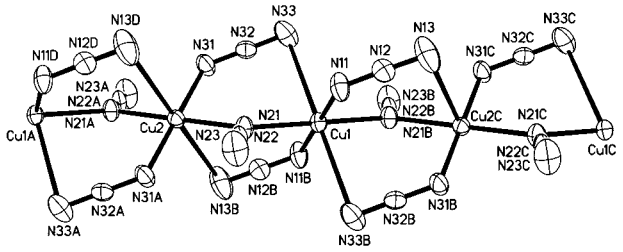

Figure 1. $[N(CH_3)_4][Cu(N_3)_3]$ (**1**): ORTEP drawing (40% ellipsoid probability) of the copper−azido chain with the atom-labeling scheme. Symmetry codes: (A) $-1-x, 1-y, 1-z$; (B) $-x, 1-y, 1-z$; (C) $1+x, y, z$; (D) $-1+x, y, z$.

Results and Discussion

Description of the Structure of $[N(CH_3)_4][Cu(N_3)_3]$ (1). The structure of this compound consists of chains of copper(II) ions and tetramethylammonium countercations. In these chains, the Cu(II) ions are simultaneously bridged by one EO and two EE azido bridges. The coexistence of both types of bridges is an extraordinarily rare phenomenon due to the very different distances involving each type of bridging. The usual intramolecular metal distances for double EE (5.5 Å) and EO (3.5 Å) bridges must be shorter and larger, respectively. This fact would cause a remarkable distortion in the coordination polyhedron around the metal, which is possible for only very few metals, in particular the copper(II) ion. For compound **1**, the Cu···Cu intramolecular separation was 3.737(1) Å. A perspective view of the molecule with the labeling of the atoms is shown in Figure 1. There are two nonequivalent copper(II) ions in the structure, which are located on inversion centers. Each copper(II) ion is bonded to six nitrogen atoms belonging to six azido groups,

(11) Walker, N.; Stuart, D. *Acta Crystallogr.* **1983**, *A39*, 158.
(12) Sheldrick, G. M. SHELXS-86. *Acta Crystallogr.* **1990**, *A46*, 467.
(13) Sheldrick, G. M. SHELX-76: A Program for Crystal Structure Determination. University of Cambridge, U.K., 1976.
(14) Sheldrick, G. M. SHELXL-93. *J. Appl. Crystallogr.* **1996**.
(15) *International Tables for X-ray Crystallography*; Kynoch: Birmingham, U.K., 1974; Vol. IV, p 99.

Table 2. Selected Bond Distances (Å) and Angles (deg) for $[N(CH_3)_4][Cu(N_3)_3]$[a]

Cu(1)−N(11)	1.968(6)	N(11)−N(12)	1.175(7)
Cu(1)−N(21)	2.036(5)	N(12)−N(13)	1.165(9)
Cu(1)−N(33)	2.789(7)	N(21)−N(22)	1.200(10)
Cu(2)−N(21)	2.047(5)	N(22)−N(23)	1.155(11)
Cu(2)−N(31)	1.961(6)	Cu(1)···Cu(2)	3.737(1)
Cu(2)−N(13B)	2.842(8)		

N(11)−Cu(1)−N(21)	88.8(2)	Cu(1)−N(33)−N(32)	89.7(5)
N(11)−Cu(1)−N(33)	92.2(3)	Cu(2)−N(21)−N(22)	113.4(4)
N(21)−Cu(1)−N(33)	84.9(2)	Cu(2)−N(31)−N(32)	122.8(5)
N(21)−Cu(2)−N(31)	90.9(2)	Cu(2)−N(13B)−N(12B)	89.7(5)
N(21)−Cu(2)−N(13B)	84.0(2)	Cu(1)−N(21)−Cu(2)	132.5(3)
N(31)−Cu(2)−N(13B)	87.2(3)	N(11)−N(12)−N(13)	174.1(10)
Cu(1)−N(11)−N(12)	123.5(5)	N(21)−N(22)−N(23)	179.3(12)
Cu(1)−N(21)−N(22)	114.1(4)	N(31)−N(32)−N(33)	177.2(8)

[a] Symmetry transformation used to generate equivalent atoms: B = $-x$, $1-y$, $1-z$.

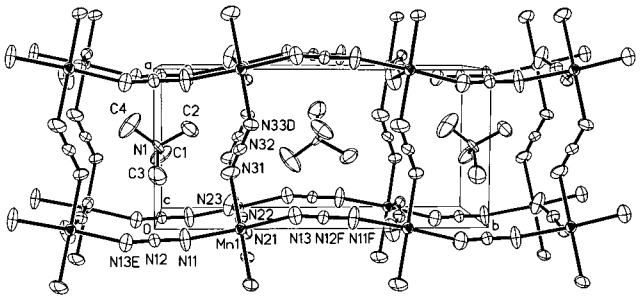

Figure 2. $[N(CH_3)_4][Mn(N_3)_3]$ (**2**): ORTEP cell plot (40% ellipsoid probability) with the atom-labeling scheme. Symmetry codes: (D) $x+1$, y, z; (E) $-x$, $y-{}^1/_2$, $-z$; (F) $-x$, $y+{}^1/_2$, $-z$. Hydrogen atoms are omitted.

four acting as EE bridging ligands and the other two as EO bridging ones. Both types of coordination polyhedra can be described as elongated octahedra, with two axial distances [Cu(1)−N(33)] of 2.789(7) Å and four equatorial ones [Cu(1)−N(11), Cu(1)−N(21)] of 1.968(6) and 2.036(5) Å for the Cu(1) polyhedron and two axial distances [Cu(2)−N(13B)] of 2.842(8) Å and four equatorial ones [Cu(2)−N(21), Cu(2)−N(31)] of 2.047(5) and 1.961(6) Å for the Cu(2) polyhedron. The large asymmetry of the Cu−N distances corresponding to the EE bridges seems to be necessary for the accommodation of the N_3 ligand in the short Cu···Cu distance. Selected bond distances and angles for this complex are given in Table 2. The bridging angle corresponding to the EO azido bridge is Cu(1)−N(21)−Cu(2) = 132.5(3)°, which is the largest one observed so far for this kind of bridging. For the EE bridges, these angles are Cu(1)−N(11)−N(12) = 123.5(5)°, N(12B)−N(13B)−Cu(2) = 89.7(5)° [B = $-x$, $1-y$, $1-z$], Cu(2)−N(31)−N(32) = 122.8(5)°, and N(32)−N(33)−Cu(1) = 89.7(5)°. The distortion of the octahedral geometry has been evaluated using the Muetterties and Guggenberger description[16] to give a Δ value near 0.26 (Supporting Information), which indicates a high distortion from the ideal topology.

The azide groups are practically linear [N(11)−N(12)−N(13) = 174.1(10)°, N(21)−N(22)−N(23) = 179.3(22)°, N(31)−N(32)−N(33) = 177.2(8)°]. The packing in the structure of **1** may be described as a "honeycomb-like" arrangement where each of the copper−azido chains is surrounded by six columns of the $[N(CH_3)_4]^+$ counterions as next neighbors and subsequently by six further Cu−azido chains (orientation along the *a* axis of the unit cell). The shortest intermolecular Cu···Cu separation is 10.312(1) Å.

Table 3. Selected Bond Distances (Å) and Angles (deg) for $[N(CH_3)_4][Mn(N_3)_3]$[a]

Mn(1)−N(11)	2.214(14)	Mn(1)−N(13)	2.221(16)
Mn(1)−N(21)	2.201(12)	Mn(1)−N(23b)	2.259(9)
Mn(1)−N(31)	2.244(13)	Mn(1)−N(33)	2.211(10)

N(11)−Mn(1)−N(13)	175.4(9)	N(13)−Mn(1)−N(33)	92.7(6)
N(11)−Mn(1)−N(21)	85.6(6)	N(21)−Mn(1)−N(23B)	176.0(6)
N(11)−Mn(1)−N(23B)	90.4(6)	N(21)−Mn(1)−N(31)	91.4(4)
N(11)−Mn(1)−N(31)	90.8(6)	N(21)−Mn(1)−N(33)	89.5(5)
N(11)−Mn(1)−N(33)	89.5(6)	N(31)−Mn(1)−N(33)	179.1(10)
N(13)−Mn(1)−N(21)	90.3(7)	N(31)−Mn(1)−N(23B)	89.4(5)
N(13)−Mn(1)−N(23B)	93.6(6)	N(33)−Mn(1)−N(23B)	89.8(5)
N(13)−Mn(1)−N(31)	87.1(6)		

[a] Symmetry transformation used to generate equivalent atoms: B = x, y, $z-1$.

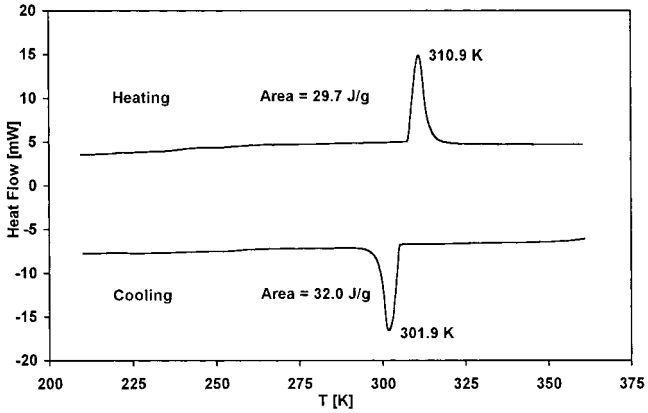

Figure 3. DSC scans for $[N(CH_3)_4][Mn(N_3)_3]$ (**2**).

Description of the Structure of $[N(CH_3)_4][Mn(N_3)_3]$ (2). The room-temperature crystal structure of this compound can be described as a distorted Perovskite-like structure; i.e., the Mn^{II} is approximately shifted from the origin of the unit cell by 0.25 along the *b* axis (Figure 2). The azido ions act as EE bridging ligands between the metals to form the three-dimensional network. A similar disposition has been observed for the related Ca(II) compound.[17] Each manganese ion shows a slightly distorted octahedral coordination sphere.[10b] The $[N(CH_3)_4]^+$ cations are located within the holes formed by the manganese(II)−azido sublattice (Figure 2). Selected bond distances and angles for this complex are given in Table 3. At approximately 305 K, the compound undergoes a reversible phase transition.

The Structural Phase Transition in Compound 2. Calorimetric Data. DSC analysis showed an exothermic sharp peak at 301.9 K during the cooling measurements, as well as an endothermic peak at 310.9 K during the heating measurements, as can be seen in Figure 3. The calculated enthalpies are −32.0 and 29.7 J/g for the cooling and heating processes, respectively. The process is reversible, indicating thermal hysteresis.

X-ray Powder Data. The X-ray powder diffraction spectra for compound **2** were recorded above and below the transition temperature (305 K). The obtained spectra correspond to the monoclinic and pseudocubic phases at low and high temperatures, respectively. These spectra are deposited as Supporting Information. The thermal variation of the lattice parameters for compound **2**, shown in Figure 4, was obtained through different measurements, in the range 20−350 K. These parameters are

(16) Muetterties, E. L.; Guggenberger, L. J. *J. Am. Chem. Soc.* **1974**, *96*, 1748.

(17) Mautner, F. A.; Krischner, H.; Kratky, C. *Monatsh. Chem.* **1988**, *119*, 1245.

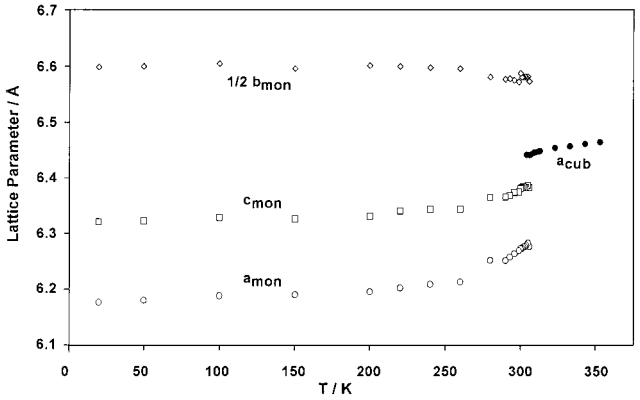

Figure 4. Temperature dependence of the lattice parameters for $[N(CH_3)_4][Mn(N_3)_3]$ (**2**).

practically constant from 20 to 200 K. Above this temperature, *a* and *c* slowly increase while $^1/_2b$ is observed to slowly decrease. The transition can be clearly noted by considering the evolution of the three parameters in the monoclinic phase (below 305 K) toward a single *a* parameter of the high-temperature phase. The cell length of the pseudocubic HT phase at 310 K is 6.446(4) Å, with one formula per unit cell. The structure of the HT phase has not yet been solved.

Infrared Spectroscopy. The most important aspects concerning the infrared spectra of compounds **1** and **2** deal with the possibility of characterizing the different coordination modes for the azido ligands.

The $\nu_{as}(N_3)$ stretching mode of the azido ion, located at approximately 2000 cm^{-1}, is very useful for determining the nature of the coordination modes of this group. In the same way, the presence of the $\nu_s(N_3)$ vibration mode is related to the existence of terminal or EO bridged azides, not appearing for the EE bridging mode. For compound **1**, the $\nu_{as}(N_3)$ stretching vibration of the azido group appears as a doublet at 2100, 2075 cm^{-1}, indicating the existence of EE bridges. This fact, together with the presence of a weak band at about 1300 cm^{-1} corresponding to the $\nu_s(N_3)$ vibration mode, supports the presence of both end-to-end and end-on azido bridges, as confirmed by the crystallographic structure for the compound.[18]

For compound **2**, the $\nu_{as}(N_3)$ stretching vibration of the azido group appears as a doublet at 2105, 2065 cm^{-1} and no $\nu_s(N_3)$ vibration mode is observed. These facts are in accordance with the existence of slightly distorted EE azido bridges and the absence of EO bridges, as observed in the crystal structure.

EPR Spectra and Magnetic Properties. The X-band EPR room-temperature spectra show a quasi-Lorentzian signal with an average *g* value of 2.10 for compound **1** and an isotropic signal with $g = 2.00$ for compound **2**, in good agreement with the octahedral environments of the Cu^{II} and Mn^{II} ions in both structures. For compound **2**, several EPR spectra have been recorded at different temperatures to follow the magnetic behavior and to observe the structural phase transition. Figure 5 shows the thermal variations of both the *g* factors and the line widths (Γ) of the different spectra after fitting to Lorentzian line shapes. As can be observed, the *g* factors are practically constant within the whole temperature range, with an average value of 2.0014. In contrast, the homogeneous variation of the line widths shows a discontinuity at 305 K, where the phase transition takes place. These results imply that no appreciable changes take place upon the distortion of the Mn octahedra.

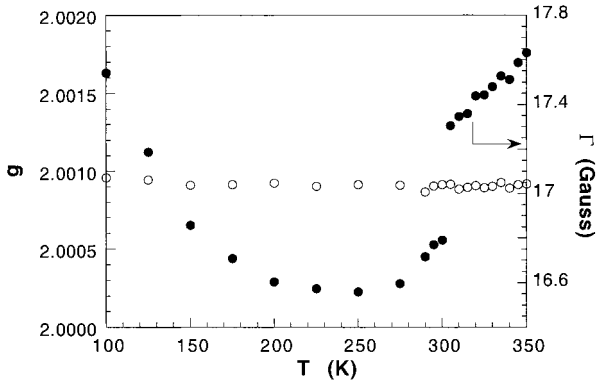

Figure 5. Variations of both the *g* factor and the line width for $[N(CH_3)_4][Mn(N_3)_3]$ (**2**) with temperature.

The sudden decrease in the line width could be caused by a slight increase in the exchange coupling constant upon passing from the high-temperature to the low-temperature phase.

The thermal variation of the molar magnetic susceptibility χ_m for compound **1** shows that χ_m values (1.93×10^{-3} cm^3 mol^{-1} (SI units: 2.43×10^{-8} m^3 mol^{-1}) at 210 K) continuously increase upon cooling. The χ_m^{-1} and $\chi_m T$ vs *T* curves for this compound are shown in Figure 6. The $\chi_m T$ values decrease with decreasing temperature from 0.41 cm^3 K mol^{-1} (SI units: 5.15×10^{-9} m^3 K mol^{-1}) (210 K) to 0.34 cm^3 K mol^{-1} (SI units: 4.27×10^{-9} m^3 K mol^{-1}) (12 K), where the curve reaches a minimum. At temperatures below this minimum, $\chi_m T$ increases again.

The magnetic behavior of compound **1**, at temperatures above 12 K, has been analyzed using the Heisenberg model for exchange interaction between pairs of Cu(II) ions with $\mathbf{S}_i$ and $\mathbf{S}_j$ spins of the form

$$H = \sum_{i>j} -2J_{ij}\mathbf{S}_i\mathbf{S}_j$$

where the existence of interactions between nearest neighbor copper ions on a chain are assumed (i.e., $J_{ij} = j$ for $j = i \pm 1$ and $J_{ij} = 0$ otherwise). The variation of the magnetic susceptibility with temperature for this compound can satisfactorily be fitted to the empirical function introduced by Hall[19] to represent the numerical calculations performed by Fisher[20] describing a uniformly spaced chain of spins with $S = {}^1/_2$:

$$\chi = \frac{Ng^2\beta^2}{kT}\left[\frac{A + Bx + Cx^2}{1 + Dx + Ex^2 + Fx^3}\right] \qquad (1)$$

where $x = J/kT$, *N* is Avogadro's number, *k* is the Boltzmann constant, β is the Bohr magneton, $A = 0.250$, $B = 0.149\,95$, $C = 0.300\,94$, $D = 1.9862$, $E = 0.688\,54$, and $F = 6.0626$.

The best fit leads to $J/k = -3.6$ K (see Figure 6). The value of $g = 2.10$ obtained from the EPR measurements was used for expression 1. The agreement factor (defined as $SE = [\Phi/(n-K)]^{1/2}$, where *n* is the number of data points, *K* is the number of adjustable parameters (1), and $\Phi = \Sigma[\chi_m T_{obs} - \chi_m T_{calc}]^2$ is the sum of squares of the residuals) using the above expression was 3.9×10^{-4}, which actually corresponds to an excellent experiment−theory agreement. Considering the structural features, the observed $J = -3.6$ K value can be explained on the basis of the possible exchange pathways present in this compound. The

(18) Lever, A. B. P.; Mantovani, E.; Ramaswamy, B. S. *Can. J. Chem.* **1971**, *49*, 1957.

(19) Hall, J. W. Ph.D. Thesis, North Carolina University. Cited by: Hatfield, W. H. *J. Appl. Phys.* **1981**, *52*, 1985.

(20) Fisher, M. E. *Am. J. Phys.* **1964**, *32*, 343.

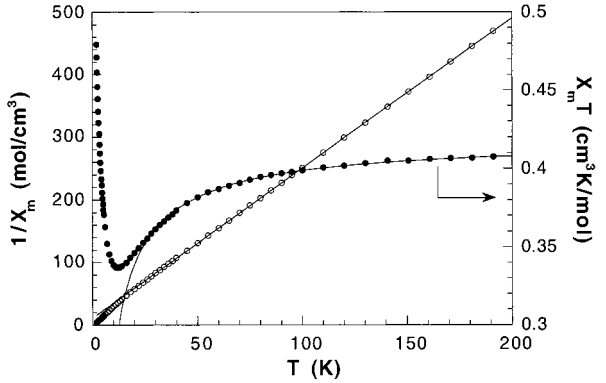

Figure 6. Thermal variations of the reciprocal magnetic susceptibility ($1/\chi_m$) and $\chi_m T$ product for $[N(CH_3)_4][Cu(N_3)_3]$ (**1**). The solid line represents the best fit curve according to the model used.

symmetric EE azido bridges, with both short Cu−N distances, usually give rise to strong antiferromagnetic interactions. However, the axial−equatorial disposition of the EE azido bridges in this compound, with long−short Cu−N distances, respectively, can lead to a negligible or very weakly antiferromagnetic contribution to the exchange mechanism.[1,21] On the other hand, the EO azido bridges usually lead to ferromagnetic interactions, but for angles greater than 108°, antiferromagnetic interactions have been observed to occur.[22,23] Therefore, the bridging angle of 132.5° in compound **1** (which is the greatest observed so far) could give rise to antiferromagnetic interactions. In this way, the EO azido bridges can be considered as the more efficient pathway, owing to the different orientations of the coordination spheres of the two neighboring Cu(II) ions, and the responsibles of the observed antiferromagnetic *J* value.

To study the possible presence of field-dependent phenomena or remanent effects associated with the increase of $\chi_m T$ below 12 K, magnetization measurements were performed at 5 K. The results did not show any indication of three-dimensional ordering.

The global $\chi_m T$ vs *T* curve looks like that of a ferrimagnetic chain (Figure 6). The existence of a ferromagnetically coupled impurity was previously discarded on the basis of elemental analysis, ICP, pattern matching, EPR, and the fact that the samples used were ground crystals. We must also take into account that, in compound **1**, $S_A = S_B$ and no unusual combination of *J* values occurs, such as that observed for $[Cu(3\text{-}Clpy)_2(N_3)_2]_n$,[24] in which one J_{AF} is followed by three J_F's and so on, where $J_{AF} > J_F$. This fact may result from the noncompensation between the local magnetic moments of the two crystallographically different copper(II) ions. The origin of this noncompensation could arise from the different orientations of two neighboring local **g** tensors in the compound. To test this hypothesis, single-crystal susceptibility measurements are needed. However, due to the too small size and the needle form of the obtained single crystals, these measurements are unfeasible. Attempts were made also to record single-crystal EPR spectra but no signals were detected.

The thermal variations of the magnetic susceptibility, in the forms of χ_m and $\chi_m T$ vs *T*, for compound **2** are shown together in Figure 7. The χ_m value increases as the temperature decreases (Figure 7), reaching a sharp maximum (11.45×10^{-3} cm^3 mol^{-1} (SI units: 1.44×10^{-7} m^3 mol^{-1})) at about 70 K, and then decreases with further cooling. At 0 K, a value of two-thirds of the susceptibility maximum can be extrapolated. A three-dimensional antiferromagnetic behavior can be deduced by considering this fact and the sharp maximum on the χ_m curve. Indeed, single-crystal experiments, a.c. susceptibility, and neutron diffraction should be necessary in order to unambiguously confirm the onset of a 3-D ordering. The $\chi_m T$ value at room temperature is 3.43 cm^3 K mol^{-1} (SI units: 4.31×10^{-8} m^3 K mol^{-1}) (Figure 7), a smaller value than that expected for an uncoupled Mn^{II} ion. This value decreases with decreasing temperature, tending to zero. A global antiferromagnetic behavior should be concluded from the magnetic measurements as shown in Figure 7. This behavior is clearly associated with the great ability of the EE azido bridges to transmit antiferromagnetic interactions. The low−high temperature (305 K) structural phase transition can be detected in this curve. This change in the strength of *J* could be caused by slight changes in the Mn−N_3−Mn bridging angles in the high-temperature phase.

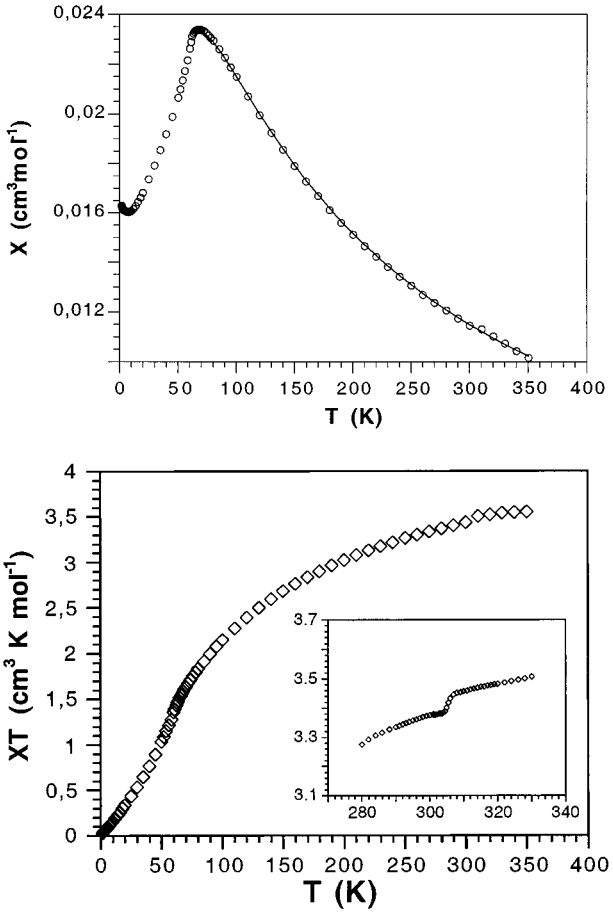

Figure 7. Thermal variation of the magnetic susceptibility (χ_m) and $\chi_m T$ for $[N(CH_3)_4][Mn(N_3)_3]$ (**2**). The solid line represents the best fit curve according to the model used.

The magnetic behavior of this compound must be explained by assuming a regular three-dimensional network, as indicated by the crystal structure. The expression of the magnetic susceptibility for a simple cubic Heisenberg antiferromagnetic system was derived from the high-temperature series expansion (HTS) model developed by Rushbrooke and Wood.[25] Consider-

(21) Bkoeche-Waskman, I.; Sikorav, S.; Kahn O. *J. Crystallogr. Spectrosc. Res.* **1983**, *13*, 303.
(22) Thompson, L. K.; Tandon, S. S.; Manuel, M. E. *Inorg. Chem.* **1995**, *34*, 2356.
(23) Escuer, A.; Vicente, R.; El Fallah, M. S.; Goher, M. A. S.; Mautner, F. A. *Inorg. Chem.* **1995**, *34*, 2356.
(24) Escuer, A.; Vicente, R.; El Fallah, M. S.; Goher, M. A. S.; Mautner, F. A. *Inorg. Chem.* **1998**, *37*, 4466.
(25) Rushbrooke, G. S.; Wood, P. J. *Mol. Phys.* **1958**, *1*, 257.

ing the exchange Hamiltonian $H = -2J\sum_{i\neq j} S_i S_j$, the following susceptibility expression was obtained:

$$\chi = \frac{35Ng^2\beta^2}{12kT}(1 + C_1x + C_2x^2 + C_3x^3 + C_4x^4 + C_5x^5 + C_6x^6) \quad (2)$$

where $x = J/kT$, $C_1 = 35$, $C_2 = 221.67$, $C_3 = 608.22$, $C_4 = 26\,049.66$, $C_5 = 210\,986$, and $C_6 = 8\,014\,980$. The rest of the symbols have their usual meanings for an $S = {}^5/_2$ system.

The preceding expression is only valid down around the maximum (paramagnetic region). The solid line in Figure 7 shows the best least-squares fitting of the susceptibility data for $[N(CH_3)_4][Mn(N_3)_3]$ using eq 2. The obtained parameters are $J/k = -2.5$ K and $g = 2.01$. The g value is in good agreement with that observed for EPR measurements.

Concluding Remarks

The same synthetic method aimed at originating three-dimensional connections of Cu(II)− and Mn(II)−azido systems has led to different one- and three-dimensional networks for copper(II) and manganese(II) species, respectively. In the former system, the copper(II) ions are simultaneously connected through one end-on and two end-to-end azido bridges, whereas in the latter, EE azido bridges connect the manganese(II) ions to form a perovskite-like three-dimensional network which undergoes a structural phase transition toward a pseudocubic ($a = 6.446(4)$ Å) phase. For both compounds **1** and **2**, antiferromagnetic couplings are observed. For compound **2**, this result is in good agreement with the existence of EE azido bridges, while for compound **1**, it should be associated with the EO azido bridge. It is worth mentioning that the large bridging angle observed for the EO azido bridges (132.5°) in this compound is responsible for the existence of the antiferromagnetic interactions. In fact, the obtained J value would not be the expected coupling for an interaction through two very weak antiferromagnetic pathways and one ferromagnetic pathway. The weak ferromagnetism observed for compound **1** at temperatures below 12 K can be associated with a noncompensation between the local magnetic moments of the copper(II) ions in the chains.

Acknowledgment. F.A.M. thanks Prof. Ch. Kratky (University of Graz, Austria) for the use of experimental equipment and Dr. Ungerank (TU-Graz, Austria) for DSC measurements. This work was carried out with partial financial support from the OENB (Project 6630), the Gobierno Vasco/Eusko Jaurlaritza (Grant PI96/39), and the Universidad del País Vasco/Euskal Herriko Unibertsitatea (Grant UPV 130.310-EB234/95), which we gratefully acknowledge.

Supporting Information Available: Packing diagrams and listings of crystal data, positional parameters, anisotropic displacement parameters, bond distances and angles, torsion angles, and molar magnetic susceptibility vs temperature data. This material is available free of charge via the Internet at http://pubs.acs.org.

IC981373S